Fitness seascapes are necessary for realistic modeling of the evolutionary response to drug therapy

Eshan S. King[1], Jeff Maltas[2], Davis T. Weaver[1], Rowan Barker-Clarke[2], Julia Pelesko[2], Emily Dolson[3], and Jacob G. Scott[2,*]

[1]Systems Biology and Bioinformatics Program, School of Medicine, Case Western Reserve University, Cleveland, OH, USA
[2]Translational Hematology and Oncology Research, Cleveland Clinic, Cleveland, OH, USA
[3]Department of Computer Science and Engineering, Michigan State University College of Engineering, Lansing, MI, USA
[*]scottj10@ccf.org

ABSTRACT

A persistent challenge in evolutionary medicine is predicting the evolution of drug resistance, which is complicated further when the drug concentration varies in time and space within a patient. Evolutionary trade-offs, or fitness costs of resistance, cause the evolutionary landscape to change dramatically as the drug selective pressure changes. In this work, we show how fitness seascapes, or collections of genotype-specific dose-response curves, more accurately describe dose-dependent evolution and the arrival of drug resistance. We measure a novel empirical fitness seascape in *E. coli* subject to cefotaxime, finding substantial growth rate penalties in exchange for drug resistance. In two computational experiments we show how the fitness seascape framework may be used to model evolution in changing environments. First, we show that the probability of evolutionary escape from extinction is dependent on the rate of environmental change, aligning with prior *in vitro* results. Then, we simulate patients undergoing a daily drug regimen for an infection with varying rates of nonadherence. We find that early drug regimen adherence is critical for successfully eliminating the infection, lending evidence to a "two strike" model of disease extinction. Our work integrates an empirical fitness seascape into an evolutionary model with realistic pharmacological considerations. Future work may leverage this platform to optimize dosing regimens or design adaptive therapies to avoid resistance.

Introduction

The evolution of treatment resistance in disease agents across kingdoms, including in cancer, infectious disease, and agricultural pests, is governed by the same fundamental evolutionary laws[1]. Evolutionary medicine is a field that studies how disease agents evolve resistance within and among human hosts. Researchers within evolutionary medicine leverage knowledge of evolutionary processes to develop new treatments and improve existing paradigms[2–4]. Recently, computational studies of the evolution of resistance have been used to optimise dosing schedules *in silico*, *in vitro*, and in clinical trials[5–11].

Fitness landscapes are mappings from genotype to fitness, often used to understand, simulate, and predict evolution[12–19]. An assumption of the fitness landscape model is that, for a given landscape, the selection pressure is constant[14]. As such, canonical fitness landscapes cannot model evolution under continuously varying selection pressure, such as the rising and falling concentration of drug in a patient over time. This limitation precludes the modeling of evolutionary trade-offs, or fitness costs, where a mutant "trades" a lower growth rate in the absence of a drug in exchange for resistance at higher concentrations of the drug[20–22].

Such trade-offs across environments are common in evolutionary medicine; drug resistance mechanisms often impose metabolic burdens or impair vital functions of the organism. When the drug-selective pressure is removed, the sensitive genotype may have a higher relative fitness and the resistant genotype may go extinct[23,24]. Moreover, disease agents in a patient will never experience a constant environment – the drug concentration will vary according to the pharmacokinetic profile, dosing schedule, and spatial distribution. Fitness seascapes extend the fitness landscape model by considering a mapping from both genotype and environment (i.e. drug concentration) to fitness[1,25–29]. In this work, we model fitness seascapes as collections of genotype-specific dose-response curves. This approach permits the modeling of fitness trade-offs across a range of drug concentrations, allowing us to model the evolution of resistance with realistic pharmacological considerations.

Here, we explore the function and utility of fitness seascapes by measuring a novel empirical fitness seascape in *E. coli* and use this data to parameterise a computational model of evolution. First, using simulated fitness seascapes, we demonstrate the necessity of modeling fitness trade-offs in a changing environment by comparing a seascape with trade-offs to a naive "null" seascape. In the null seascape, we enforce a "no trade-off" condition– what one implicitly assumes when modeling evolution under varying selection with canonical fitness landscapes. Then, we measure an empirical fitness seascape in genetically engineered *E. coli*, finding evidence for pervasive fitness costs to resistance. Using this empirical fitness seascape, we model the emergence of resistance in two computational experiments. In the first, we analyze the impact of the rate of change in drug concentration on the probability of survival and resistance. In the second, we analyze the impact of drug regimen non-adherence in simulated patients on resistance and survival of infectious agent populations, finding that early drug regimen adherence is critical for successful elimination of the pathogen. Our work demonstrates that dose-response data is important for accurately modeling the emergence of resistance under varying selective pressure, which is a significant consideration for designing adaptive therapies in the context of evolutionary medicine.

Results

Fitness trade-offs shape evolutionary response to selection

We first explored the importance of evolutionary trade-offs in predicting the emergence of therapeutic resistance. Here we define evolutionary trade-offs as the difference between the rank-order of the drug-free growth rate and drug sensitivity (i.e. IC_{50}) among subspecies under study. This type of evolutionary trade-off is naturally modeled by fitness seascapes, whereas it is not intrinsically modeled by canonical fitness landscapes. To illustrate what we gain with fitness seascapes, we simulated a random "null seascape", which has a genotype fitness rank-preserving constraint, and a natural seascape, which has no such constraint (**Fig. 1**). The genotype rank order of the IC_{50} in the null seascape is the same as the rank-order of the drugless growth rates (i.e., no trade-offs are present). The null seascape represents what one implicitly assumes if modeling evolution under varying selection with a canonical fitness landscape. We then simulated evolution with both seascapes subject to changing drug concentration.

The simulated null seascape is shown in **Fig. 1A**. Owing to the rank-order preserving constraint, no fitness trade-offs are present, and the most fit genotype at low drug concentration is also the most drug resistant genotype. The simulated natural seascape is shown in **Fig. 1B**. Because there is no rank-preserving constraint, some genotypes exhibit fitness costs to resistance. For instance, the most drug resistant genotype, 11, exhibits the lowest growth rate at $10^{-3}\mu$M drug concentration. Rank-order fitness landscapes are shown for both simulated fitness seascapes at different drug concentrations (**Fig. 1 C-D**). Because the null seascape has a rank-preserving constraint, the rank-order fitness landscape does not change as a function of drug concentration. In contrast, the fitness landscape for the natural seascape exhibits 3 distinct peaks as the drug concentration changes, admitting non-stationary clonal dynamics as the concentration changes.

The rank-order preserving assumption has implications for predicting the trajectory of evolution under changing drug concentration. When simulating evolution with the null seascape (**Fig. 1E**), the wild type (00) quickly fixes at 10^{-3} μM and remains the dominant strain, even as the drug concentration steps up to 10^1 and 10^5 μM. In contrast, when simulating evolution with the natural seascape (**Fig. 1F**), the 01 mutant briefly fixes at 10^{-3} μM. Then, when the drug concentration steps up to 10^1 μM, the 00 strain becomes the most fit and subsequently takes over. Finally, at 10^5 μM, the 11 double mutant exhibits the greatest degree of resistance and fixes. The difference in the evolutionary trajectory between **Fig. 1E** and **F** illustrates the importance and utility of fitness seascapes in modeling evolution under changing drug concentration.

Empirical fitness seascapes reveal fitness trade-offs

Next, we explored fitness trade-offs in nature and generated fitness seascape data to parameterize an evolutionary model. Specifically, we sought to measure a novel fitness seascape and observe whether evolutionary trade-offs are seen. Using genetically engineered *E. coli* (see methods), we measured the cefotaxime dose-response curves for 16 genotypes (4 point mutations) representing a combinatorially complete subset of the β-lactamase gene. The resulting fitness seascape is shown in **Fig. 2**. All dose-response curve fits are shown in **Fig. S1**. We compared our IC_{50} to the minimum inhibitory concentration (MIC) reported by Weinreich et al.[12] for the same *E. coli* strains, finding a roughly linear relationship (**Fig. S2**). Deviations between these experiments are most likely due to different drug concentration gradients used and the continuous nature of IC_{50} versus discrete MIC.

As hypothesized, we found evolutionary costs to resistance. For instance, the triple and quadruple mutants, 0111 and 1111, are highly drug resistant relative to the other strains. However, they both incur a fitness cost at low concentrations of the drug, as shown by a lower growth rate at 10^{-3} μg/mL compared to less resistant strains, such as 0000 (wild-type). Fitness landscapes, calculated as the rank-order growth rate of the 16 genotypes at three different drug concentrations, are plotted above the dose-response curves. Two distinct peaks are visualized in these fitness landscapes: genotype 0011 at $10^{-2.5}$ μM and 10^0 μg/mL and 0111 at $10^{2.5}$ μg/mL. We also visualized fitness trade-offs by plotting the drug-free growth rate versus IC_{50} for

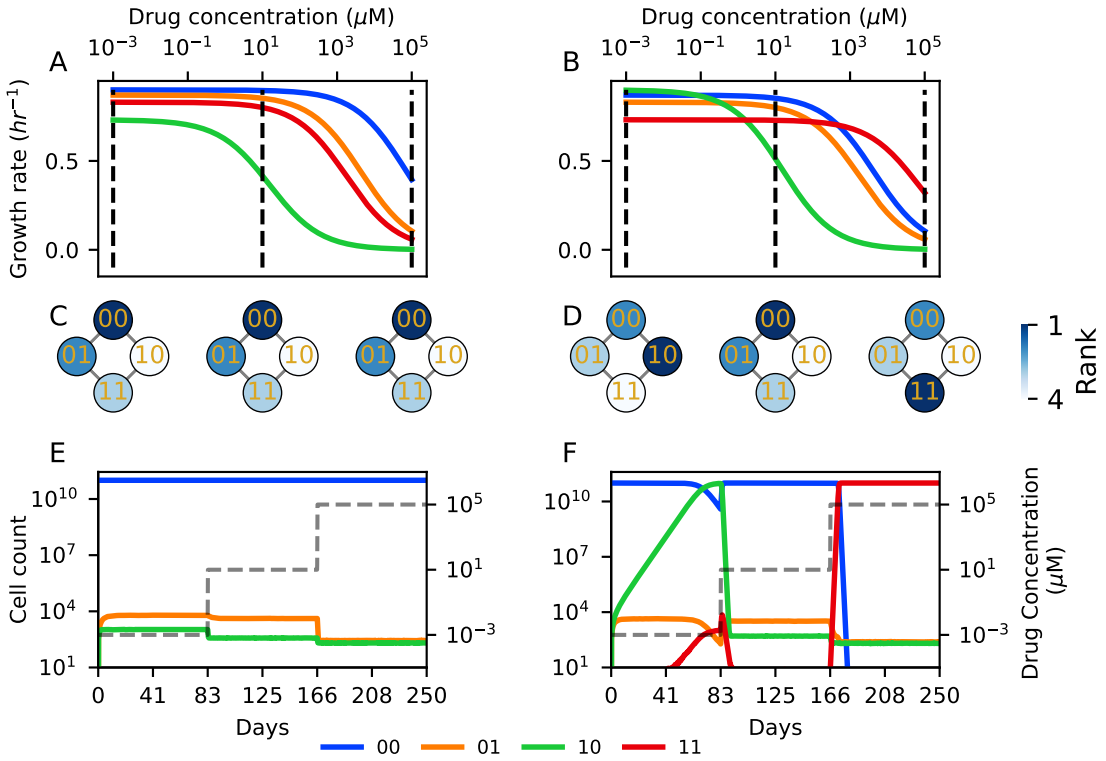

Figure 1. **Evolutionary trade-offs affect evolutionary simulations under changing drug concentrations.** (**A**) Simulated fitness seascape generated with a genotype rank-preserving constraint (null seascape). Fitness landscapes are shown based on the genotype rank-order at the drug concentration given by the black vertical dotted lines. The genotype rank-order of the null seascape is the same as the rank-order of the natural seascape at drug concentration of 10 μM. (**B**) Simulated fitness seascape with no rank-preserving constraint (natural seascape). Genotype rank-order and landscape topography change several times across drug concentration increases. (**C-D**) Landscapes corresponding to the genotype-rank order at three different drug concentrations (10^{-3}, 10^{1}, and 10^{5} μM) for the null seascape (**C**) and natural seascape (**D**). (**E**) Evolutionary simulations with the null seascape in (**A**) subject to 3 step changes in drug concentration (average of 10 simulations). Grey dotted line represents the drug concentration through time. (**F**) Evolutionary simulations with the natural seascape in (**B**) subject to 3 step changes in drug concentration (average of 10 simulations).

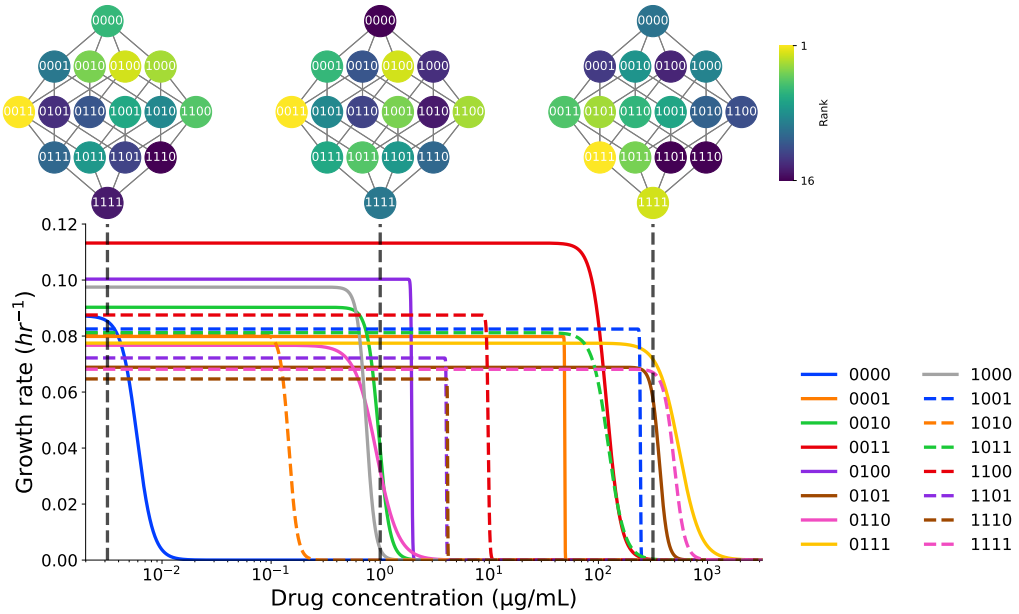

Figure 2. ***E. coli* fitness seascape reveals fitness trade-offs.** Novel fitness seascape for *E. coli* engineered with a combinatorially complete set of resistance mutations in the β-lactamase gene subject to cefotaxime. Different colors and dotted vs. solid lines represent the 16 genotypes quantified. Fitness landscapes above show the rank-order fitness of genotypes at drug concentrations specified by the vertical dotted lines.

each genotype, finding a roughy inverse relationship (**Fig. S3**). A significant outlier is genotype 3 (0011), which has both a high drug-free growth rate and a high IC_{50}. Genotype 3 possibly represents the impact of a compensatory mutation: genotype 3 has roughly the same level of resistance as genotype 1 (0001), but the addition of a second mutation rescues the drug-free growth rate. Nonlinear epistasis such as this is difficult to predict but is important to understand when modeling the evolution of resistance.

Increasing rates of change in drug concentration result in a lower probability of resistance

To further explore the importance and utility of fitness seascapes in modeling the emergence of drug resistance with realistic pharmacokinetic considerations, we performed two computational experiments using the empirical fitness seascape shown in **Fig. 2**. For these simulations, the growth rates were scaled so that the maximum drug-free growth rate in the fitness seascape was 1 replication per hour. In the first experiment, we observed the effect of different rates of change in drug concentration on the probability of evolutionary escape (i.e., probability of resistance). We sought to replicate the basic structure of experiments by Lindsey et al., where they investigated the impact of rate of change in drug concentration on the probability of evolutionary escape *in vitro*[30]. We simulated passaging cells daily by dividing the population size by 40 every 24 hours and increasing the drug concentration according to the prescribed environmental rate of change. An overview of the modeling framework is shown in **Fig. 3** and described in detail in the methods. Example data, including drug concentration curves and evolutionary time traces, are shown in **Fig. 4 A-D**. The daily increase in drug concentration is determined by the one-compartment pharmacokinetic model (Eq. 1) with the elimination rate k_{elim} set to 0:

$$c(t) = c_{max}(1 - e^{-k_{abs}t}). \tag{1}$$

Each simulation has a varying rate paramter k_{abs} with the same max drug concentration c_{max}. Drug concentration curves in **Fig. 4 B** and **C** are colored by the most fit genotype at the given drug concentration.

As expected from prior *in vitro* studies, a higher rate of change in drug concentration corresponded with a lower probability of survival of the infectious agent population (**Fig. 4 E**). Similarly, higher rates of change in drug concentration corresponded with lower probabilities of resistance (**Fig. 4 F-G**). Here, survival is defined as at least 1 remaining disease agent in the population, and reaching a particular resistant genotype is defined as the frequency of the genotype being at least 10% of the total population size. A rapid rate of change, $k_{abs} = 0.024$, resulted in 100% elimination of the populations, whereas a moderate rate of change, $k_{abs} = 0.02$ resulted in elimination of roughly 50% of the populations. Furthermore, when subject to a low rate of change, $k_{abs} = 0.012$, 100% of the infectious agent populations survive. Similar patterns are seen in the time-to-event (TTE) curves with the primary endpoints of single and double mutants: high rates of change result in very low rates of reaching the

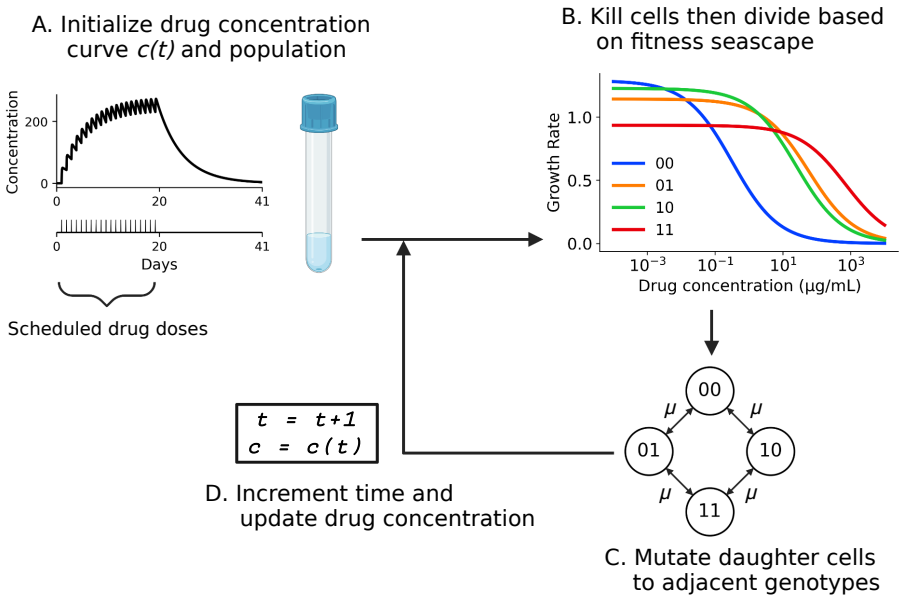

Figure 3. Overview of simulating evolution with FEArS. We developed FEArS (Fast Evolution on Arbitrary Seascapes), a software package for simulating a variety of evolutionary experiments with empirical and simulated data. To simulate evolution, a drug concentration curve and a disease agent population with user-defined parameters are initialized (**A**). Then, at each time step, cells from the population die at a constant rate and divide at a rate defined by the fitness seascape (**B**). Then, daughter cells mutate to adjacent genotypes at a constant mutation rate μ (**C**). Finally, the time step is incremented and the current drug concentration is updated (**D**). The drug concentration curve in (**A**) represents the serum drug concentration of a patient taking a daily oral antibiotic regimen, with doses administered indicated by vertical lines below the x-axis.

resistant genotypes, whereas moderate rates of change result in a moderate probability of resistance and low rates of change result in 100% resistance. Single and double mutants were chosen as aggregate endpoints because of the heterogeneity in evolutionary trajectories between simulations. These results align closely with the aforementioned *in vitro* study in *E. coli* subject to rifampicin by Lindsey et al.[30].

Increasing rates of drug regimen non-adherence result in increasing probability of resistance, while adherence early in the infection is associated with a greater likelihood of eliminating the infection

Patient drug regimen nonadherence is a common hindrance to effective antibiotic therapy and may contribute to drug resistance[31,32]. Indeed, nonadherence may be common even in short-term antibiotic therapy regimens[33]. To test the effects of varying levels of drug regimen nonadherence on the probability of therapy resistance with fitness seascapes, we simulated a population of patients undergoing a drug regimen to treat an infection. Simulated patients underwent a daily oral antibiotic regimen with a fixed probability of "forgetting" to take each individual dose (p_{forget}). Pharmacokinetic drug concentration curves were generated based on each simulated patients' resulting drug dosing regimen (see Eq. 5 and 6 in methods for details). Example data are shown in **Fig. 5 A-F**. Both representative patients had the same rate of nonadherence ($p_{forget} = 0.6$), but the actualized dosing regimens are substantially different (**Fig. 5 E and F**) Importantly, as indicated by the different colors, the drug concentration curves for the representative patients traverse different genotype selection windows through time, making it difficult to predict the evolutionary path to resistance (**Fig. 5 B and D**).

Computational experiments reveal that drug regimen nonadherence has a substantial impact on the probability of survival and resistance of the infectious agent. In simulated patients with 100% adherence to the drug dosing regimen, $p_{forget} = 0.0$, less than 10% of the infectious population survives by the end of the study, whereas in very non-adherent patients, $p_{forget} = 0.8$, 100% of the infectious populations survive (**Fig. 5 G**). Similar patterns are seen in the resistance TTE curves (**Fig. 5 H and I**). Survival and resistance of the infectious agent population represents an ongoing, drug resistant infection in a simulated patient.

We next sought to understand whether there were specific patterns in the dosing regimens between patients who successfully eliminated their infections and patients whose infections became resistant. Interestingly, we discovered 3 distinct regimens of dose importance depending on the individual patient's rate of nonadherence (**Fig. 6**, top row). For patients with very high rates of nonadherence ($p_{forget} = 0.8$ and 0.6), there is no substantial difference in the importance of individual doses. However, for patients with a moderate rate of nonadherence ($p_{forget} = 0.4$), doses 2, 3, and 4 are particularly important. These doses are significant compared to dose 1 because, prior to the first administered dose, there is no selection on drug resistance. However, after the first administered dose, the subsequent doses are critical for eliminating the pathogen before drug resistant clones can

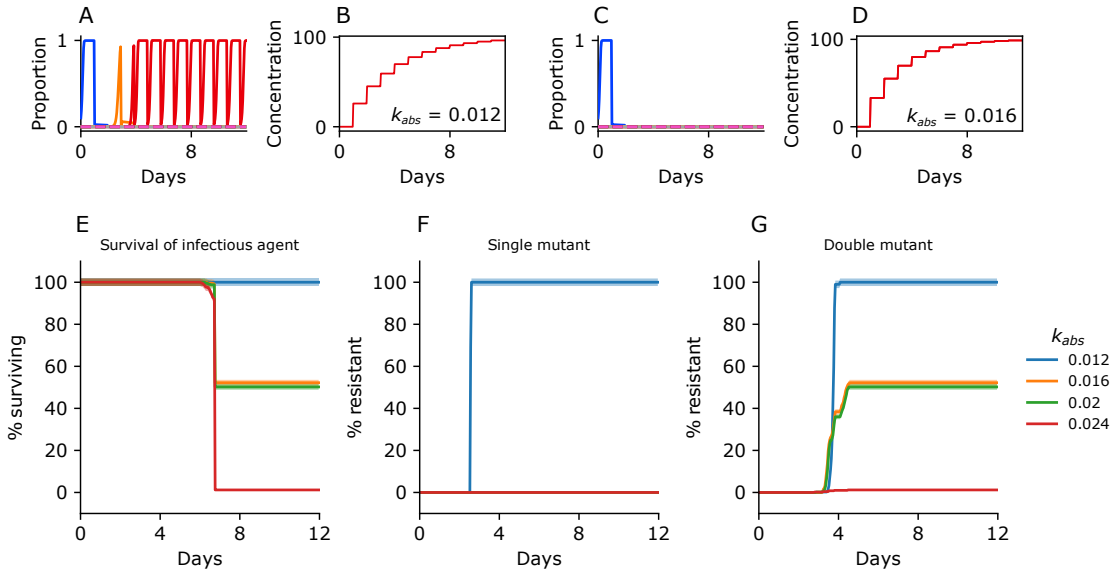

Figure 4. Differing rates of change in drug concentration result in different rates of survival and resistance of the infectious agent population. **(A-D)** Example evolutionary time traces and corresponding drug concentration curves. **(A)** Example evolutionary time trace of a population that escaped extinction and became resistant. Different colors represent different genotypes. Blue, orange, and red represent genotypes 0000, 0001, and 0011, respectively. **(B)** Drug concentration curve corresponding to **(A)** (k_{abs} = 0.012 hr^{-1}). The drug concentration is increased when the cells are passaged every 24 hours. **(C)** Evolutionary time trace of a population that went extinct. **(D)** Drug concentration curve corresponding to **(C)** (k_{abs} = 0.016 hr^{-1}). **(E-G)** TTE curves of survival and extinction of infectious agent populations. **(E)** TTE curves of survival of the infectious agent population under different rates of change in drug concentration (k_{abs}). **(F)** TTE curves with the endpoint defined as the population evolving to any single mutant. **(G)** TTE curves with the endpoint defined as the population evolving to any double mutant. k_{abs} given in units of hr^{-1}. Survival is defined as at least 1 surviving infectious agent remaining within a patient. Resistance is defined as the population of the resistant genotype being at least 10% of the carrying capacity. Error bands around TTE curves are the standard deviation of the estimator. $N = 500$ per k_{abs}.

proliferate. Patients who eliminated their infection were twice as likely to correctly take their scheduled dose on day 2 of their regimen, indicating that early drug regimen adherence is critical for avoiding drug resistance in this regime. Finally, for highly adherent patients ($p_{forget} = 0.2$), the second dose alone is important for successfully eliminating the infection. The relative importance of doses 3 and 4 are reduced at this level of nonadherence because the probability of taking the first dose is 0.8, and the probability of taking either of the first two scheduled doses is 0.96. To further explore this effect, we analyzed the impact of the time between the first two doses on treatment outcome, finding that the vast majority of successful regimens had 1 day between the first two administered doses (**Fig. 6**, bottom row). Only 3 out of 1,375 successful regimens had 2 days between the first two doses, and none had more than 2. In contrast, regimens that failed to eliminate the infection had far more variable times between the first two doses. Together, these results suggest that there is a narrow window of time to administer the second dose to avoid drug resistance and drive the infectious population to extinction.

Parameter sensitivity analysis reveals model sensitivity to mutation rate and carrying capacity

To parameterize our model, we used *E. coli* death rates and mutation rates estimated from the literature (see methods). Carrying capacity choices were based on *in-vitro* experimental conditions. However, death rate is difficult to define in *E. coli*, and it is unclear how immune system interactions will affect the death rate compared to simple *in vitro* models. In addition, mutation rate varies by orders of magnitude between strains, and mutation rate may fluctuate in an individual strain as a population adapts to stress[34]. Furthermore, carrying capacity likely varies by tissue type and may also vary in time over the course of an infection. Therefore, to better understand the generalizability of our findings, we performed parameter sensitivity analysis by sweeping across different values of mutation rate, death rate, and carrying capacity using Latin Hypercube Sampling. The outcome quantified was the survival probability for a constant rate of environmental change. As shown in **Fig. S5**, mutation rate ($r = 0.65$, $p < 10^{-45}$) and carrying capacity ($r = 0.955$, $p < 10^{-76}$) both strongly correlated with survival as revealed by multiple regression analysis. On the other hand, death rate had no significant correlation with survival ($r = 0$, $p > 0.99$). Future applications of this modeling framework will require careful validation of carrying capacity and mutation rate parameters to ensure the generalizability of any results.

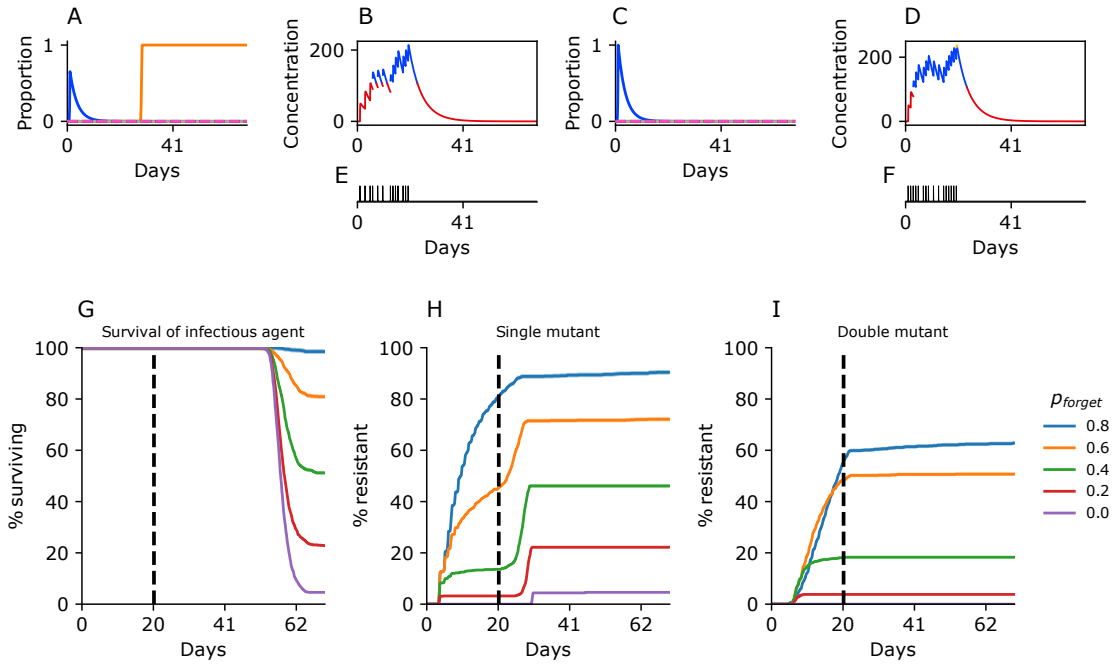

Figure 5. Increasing rates of drug regiment non-adherance result in increasing rates of resistance of the infectious agent population. (A-F) Example evolutionary time traces and corresponding drug concentration curves and drug dosing regimens. **(A)** Example evolutionary time trace of a population that escaped extinction and became resistant. Different colors represent different genotypes. Blue and orange represent genotypes 0000 and 0001 respectively. **(B)** Drug concentration curve corresponding to **(A)** ($p_{forget} = 0.6$). **(C)** Evolutionary time trace of a population that went extinct. **(D)** Drug concentration curve corresponding to **(C)** ($p_{forget} = 0.6$). **(E-F)** Corresponding drug regimens for both example simulations. Vertical lines indicate days where the simulated patients correctly took a scheduled dose. **(G-I)** TTE curves of survival and resistance of infectious agent populations. **(G)** TTE curves for survival of the infectious agent population for varying p_{forget}. **(F)** TTE curves with the endpoint defined as the population evolving to any single mutant. **(G)** TTE curves with the endpoint defined as the population evolving to any double mutant. Drug regimens were one dose of cefotaxime every 24 hours for 20 days if perfectly adherent. Vertical dotted lines indicate the end of the dosing regimen. Survival is defined as at least 1 surviving infectious agent remaining within a patient. Resistance is defined as the population of the resistant genotype being at least 10% of the carrying capacity. Error bands around TTE curves are the standard deviation of the estimator. $N = 1000$ per p_{forget}.

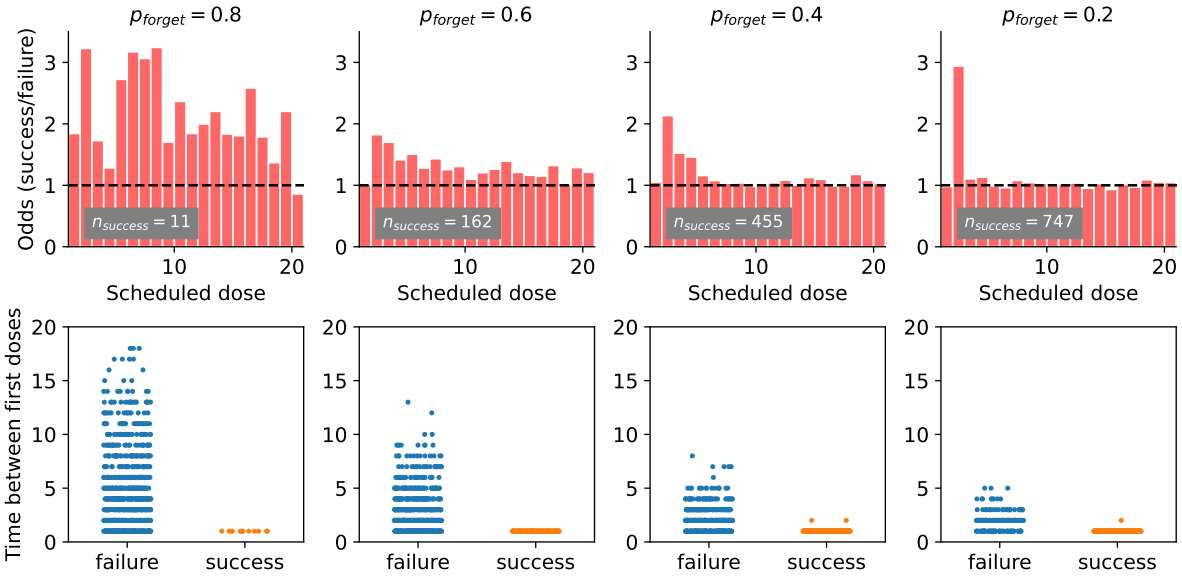

Figure 6. Early drug regimen adherence is critical to successfully eliminating the infection. Top row: Bar charts representing the odds of correctly taking a scheduled dose between patients who successfully eliminated their infection and patients whose infection became resistant (i.e. failure) for each p_{forget}. Early drug regimen adherence becomes critical as nonadherence decreases. $n_{success}$ refers to the number of disease agent populations that were successfully eliminated for each experimental condition. $N = 1000$ per p_{forget}. **Bottom row:** Time in days between the first two doses partitioned by the success or failure of the regimen for each corresponding p_{forget}.

Discussion

Predicting the evolution of drug resistance is an important step in designing adaptive therapies. In this work, we have shown how fitness seascapes may be used to integrate time-varying drug concentration curves, what one would expect to find in a patient, into a computational model to simulate evolution and predict resistance. We presented a novel fitness seascape in *E. coli*, finding evidence for pervasive fitness costs to resistance. We used this fitness seascape and a novel computational platform to investigate patterns in drug nonadherence, finding that early drug regimen adherence is critical to avoiding drug resistance.

Other empirical fitness seascapes in infectious disease exhibit similar evolutionary fitness trade-offs and rank-order changes. For instance, Ogbunugafor et al. explored adaptive fitness landscapes in engineered *Saccharomyces cerevisiae*[26] and Das et al. similarly quantified an adaptive fitness landscape in *E. coli* dosed with ciprofloxacin. Després et al. directly interrogated the effect of all single nucleotide substitutions in *S. cerevisiae* Fcy1, the target of drug 5-fluorocytosine, finding pervasive fitness trade-offs. The presence of evolutionary trade-offs in these different microbial models and drug classes is evidence of their ubiquity in infectious disease.

Our drug dosing finding is similar to other theoretical work investigating a model of Anthropocene extinction to eliminate metastatic cancer[35]. In their work, Gatenby et al. presented a "two-strike" model, where the first strike reduces the tumor size and the second strike leverages the evolutionary dynamics of small populations sizes to drive the tumor to extinction. Importantly, they identify a "window of opportunity" of time between the first and second strikes where extinction is possible. This is analogous to our finding that the timing of the second dose is critical to eliminating the infection.

A natural extension to our work is to use fitness seascapes to model evolution when the drug concentration varies in space, such as tissue drug concentration gradients within a patient that arise due to diffusion. Indeed, using a computational model, Moreno-Gamez et al.[36] showed that variable rates of drug distribution within the body may favor the evolution of resistance, and Feder et al.[37] use a similar model to explain triple drug resistance in HIV. Fitness seascapes will likely prove useful in modeling these dynamics as well when integrated into spatial models of evolution, as the selection pressures of variable drug concentrations are immediately reflected in the fitness seascape model.

Another potential extension of this work is in antibiotic cycling to avoid resistance in bacteria. Much interest has been given to optimizing antibiotic cycling in both computational studies with fitness landscapes[13,38–41], *in vitro* studies[42], and clinical trials[43]. In these models, different antibiotics are associated with different fitness landscapes. By leveraging fitness seascapes, we can greatly increase the number of possible distinct fitness landscape topographies accessible with a given set of antibiotics. Each individual drug may produce several different changes in genotype fitness rank as a function of antibiotic concentration. Furthermore, one could modulate the antibiotic dose to control evolution and avoid resistance with fitness seascapes[44]. Along with antibiotic cycling, optimizing drug dosing regimens is another natural application of our work. By varying the timing and dose of an antibiotic therapy, we may discover parameter ranges that reliably avoid resistance *in silico*. Then, using empirical knowledge of patient preferences[33,45], we may deliver dosing regimens that are both amenable to patient adherence and successful elimination of the infection.

Previous work has leveraged what is, in principle, a fitness seascape to analyze drug regimen nonadherence. For instance, Rosenbloom et al.[46] previously explored the relationship between drug regimen adherence and resistance in a computational model of HIV using a two-state model. In this case, the two states were a drug-susceptible wild-type strain and a drug-resistance mutant strain. Our study extends their experimental design into the fitness seascape model with an arbitrary number of genotypes, expanding the flexibility and tractability of this type of study without significantly increasing the complexity.

A similar platform of modeling evolution with fitness seascapes was introduced by Engelstädter[47]. Here, we have expanded on their work along several domains. First, we have developed an agent-based model of evolution on fitness seascapes, FEArS, that allows for arbitrary empirical and simulated fitness seascapes, arbitrary drug concentrations, an arbitrary number of genotypes, and a wide array of experiments and experimental parameters. Notably, FEArS models cell death, allowing the for the study of extinction versus resistance experiments, and is agent-based, allowing for the study of stochastic emergence of resistance. Furthermore, we have employed empirical fitness seascapes in our computational studies and qualitatively compared the results to *in vitro* studies. Finally, we have demonstrated the utility of fitness seascapes using an experiment with simulated patients undergoing a drug regimen nonadherence study, finding that greater rates of nonadherence result in a greater probability of resistance and that early regimen adherence is important for eliminating the pathogen.

There are several limitations to this work. First, the 4-allele fitness seascape quantified here represents only a small set of the possible resistance mutations. For instance, off-target mutations in genes regulating drug efflux pumps or cell metabolism may also contribute to resistance. A more robust method for generating genotype-fitness mappings in an unbiased way will likely be necessary for generalizing these results. Furthermore, the evolutionary model employed here only represents well-mixed *E. coli* growing *in vitro*– we do not model immune system interactions, spatial considerations, or frequency-dependent fitness effects. In addition, parameter sensitivity analysis revealed model sensitivity to mutation rate and carrying capacity. A more complete evolutionary model with carefully chosen biological parameters will be important for future clinical applications of this work.

Our work represents the first application of fitness seascapes to predicting the emergence of resistance in evolutionary

medicine. Our results suggest that explicit modeling of evolutionary trade-offs is important for predicting evolution under time-varying drug concentration, and that this modeling framework may be useful for optimizing drug dosing regimens *in silico* and designing adaptive therapies.

Methods

Estimating dose-response curves

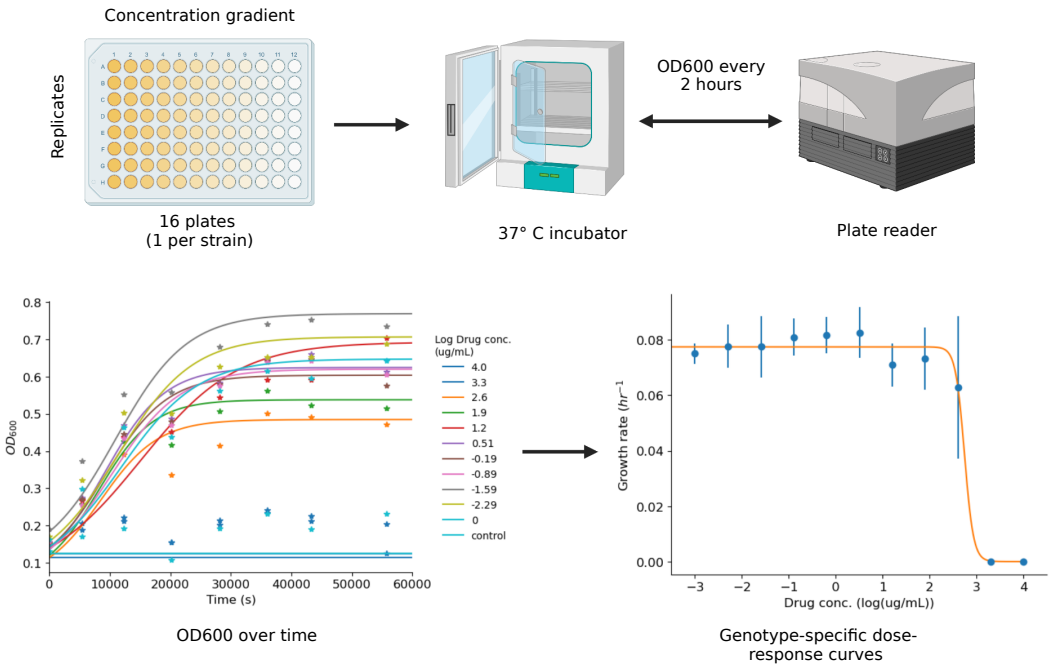

Figure 7. Fitness seascape estimation experimental overview. Strains were inoculated into 96-well plates with cefotaxime concentration gradients. Plates were incubated at 37°C and trasfered to a plate reader every 2 hours for OD600 readings. Logistic growth curves were fit to OD600 over time to estimate growth rates. Hill dose-response curves were fit to growth rate versus drug concentration data to estimate genotype-specific dose-response curves.

We measured a combinatorially complete seascape to cefotaxime using genetically engineered DH5-α *E. coli* provided to us by the Weinreich Lab at Brown University[12]. These strains have combinations of four point mutations in the β-lactamase gene. Each point mutation individually increases resistance to β-lactam antibiotics. To measure the seascapes, strains were inoculated into LB broth + 10 ug/mL tetracycline and grown up overnight in a bacterial shaking incubator set to 37°C and 225 rpm. 16 plates, one plate per genotype, were prepared with a 5-fold cefotaxime dilution scheme and one row free of antibiotic. The plates were organized such that there were 8 experimental replicates per genotype. 1 uL of bacteria was inoculated into each well, after which plates were sealed with adhesive film. Plates were then incubated at 37°C with no shaking and transferred by hand to a Tecan Spark microplate reader for OD600 readings every two hours for 20 hours. Plates were shaken at 510 rpm for 10 seconds prior to OD600 readings. Logistic growth curves adapted from Zwietering et al.[48] were fit to time-series optical density data to obtain the max growth rate per replicate, where OD_0 and OD_{max} are the initial and maximum optical density, u_{max} is the maximum growth rate, and λ is the lag time ((Eq. 2):

$$OD(t) = OD_0 + \frac{OD_{max}}{\left(1 + \exp\left[\left(\frac{4\mu_{max}}{OD_{max}}\right)(\lambda - t) + 2\right]\right)}. \tag{2}$$

Hill dose-response functions were fit to growth rate data to obtain pharmacodynamic dose-response curves , where $g_{drugless}$ and IC_{50} are the genotype-specific drugless growth rate and IC_{50}, h is the Hill coefficient, and $[c]$ is drug concentration (Eq. 2):

$$g([c]) = \frac{g_{drugless}}{1 + e^{\left(IC_{50} - log([c])\right)/h}}. \tag{3}$$

An overview of the seascape estimation process is shown in **Fig. 7**. Dose-response curve fits for each genotype are shown in **Fig. S1**. Raw data and analysis code are available in the github repository (https://github.com/eshanking/seascapes_figures).

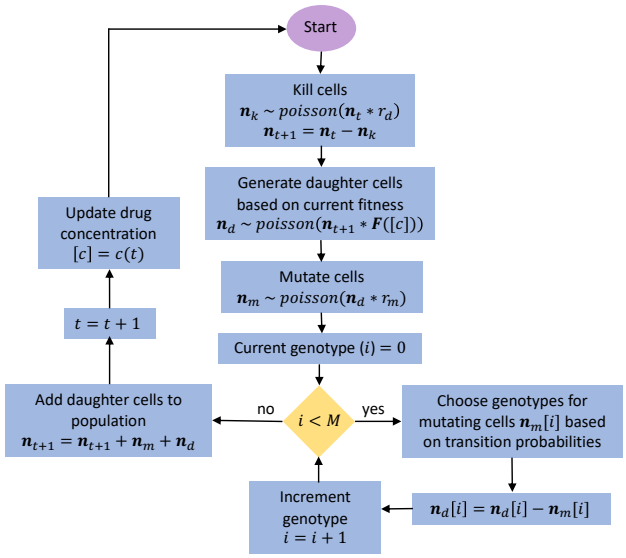

Figure 8. FEArS algorithm flow chart. n_t is a vector of genotype populations at time t, τ_d is the death rate, $F([c])$ is a vector of genotype fitness at drug concentration c, r_m is the mutation rate, and M is total number of genotypes. Cell death, division, and mutation number are modeled with the Poisson distribution. The specific mutation for each cell is chosen by picking from a uniform distribution of all possible genetic changes in the set of alleles under study. Code can be found at https://github.com/eshanking/seascapes_figures.

Computational model

We developed an agent-based algorithm, FEArS (Fast Evolution on Arbitrary Seascapes), to simulate evolution on fitness seascapes (**Fig. 8**). FEArS models carrying capacity, agent replication, mutation, death, and arbitrary drug dosing regimens. With this algorithm, genotypes are modeled as a bit string of n alleles, with 0 representing the wild type and 1 representing a point mutation at that location, yielding 2^n possible combinations. For example, in a 4-allele scenario, 0000 represents the wild type and 1111 represents the quadruple mutant. Agents mutate from one genotype to another by changing a single bit from 1 to 0 or vice-versa. In simulations, the drug concentration is updated at every time step (1 hour unless otherwise specified) according to the drug dosing regimen and the fitness of each genotype is updated according to the fitness seascape. The number of cells to die, divide, and mutate is drawn from a Poisson distribution at each time step with the argument $n * r_x$, where n is cell count and r_x is the mutation rate, death rate, or division rate. Only daughter cells are allowed to mutate. All simulations use a carrying capacity between 10^9 and 10^{11} cells. The growth rate is scaled by $1 - \frac{n}{K}$ at each time step, where n is the total number of cells and K is the carrying capacity.

Patient drug serum concentrations, $c(t)$, are modeled with a 1-compartment pharmacokinetic model:

$$c(t) = c_{max}[e^{-k_{elim}t} - e^{-k_{abs}t}], \tag{4}$$

where k_{abs} and k_{elim} represent absorption and elimination rates and c_{max} represents the maximum drug concentration. Drug doses are simulated with an impulse train, with each impulse representing a dose. Serum concentration over time for each patient is computed by convolving the drug dose impulse train with the pharmacokinetic model. Formally, this is done by generating a set (D) of numbers representing the time of each scheduled drug dose. Then, for each patient, a random subset of drug doses are removed from D, with each drug dose having a constant probability p_{forget} of being removed, resulting in the set of drug doses that the simulated patient correctly self administered (D_a). A Dirac comb is generated using D_a with the period T equal to the time between drug doses (Eq. 5):

$$III_a(t) = \sum_{d \in D_a} \delta(t - dT), \tag{5}$$

and the resulting impulse train is convolved with the pharmacokinetic model in Eq. 4 to generate the simulated patient's serum drug concentration (Eq. 6):

$$c_{patient}(t) = c(t) \circledast III_a(t). \tag{6}$$

Computational Parameters			
Parameter	Value	Citation	Sensitivity Range
Death rate	$0.0144hr^{-1}$	Gonidakis et al.[49]	0.001 to 0.1
Mutation rate	$1.4x10^{-8}$ per bp	Jee et al.[50]	10^{-9} to 10^{-7}
Cefotaxime absorption rate	$0.95hr^{-1}$	Patel et al.[51]	na
Cefotaxime elimination rate	$0.00839hr^{-1}$	Patel et al.[51]	na

Table 1. Computational parameters estimated from literature and parameter ranges used in sensitivity analysis.

Computational parameters

Death[49] and mutation[50] rates were inferred from existing literature on *in vitro E. coli* models. As these *in vitro* systems do not include immune system interactions, we expect the death rate to be much higher in the clinical setting. As such, these computational experiments represent dosing an *in vitro E. coli* culture. Cefotaxime pharmacokinetic parameters were estimated from a clinical population study[51]. Parameters and the range used in the sensitivity analysis are shown in **Table 1**.

References

1. Lässig, M., Mustonen, V. & Walczak, A. M. Predicting evolution. *Nat. Ecol. Evol.* **1**, 0077 (2017).
2. Stearns, S. C. Evolutionary medicine: Its scope, interest and potential. *Proc. Royal Soc. B: Biol. Sci.* **279**, 4305–4321, DOI: 10.1098/rspb.2012.1326 (2012).
3. Grunspan, D. Z., Nesse, R. M., Barnes, M. E. & Brownell, S. E. Core principles of evolutionary medicine. *Evol. Medicine, Public Heal.* **2018**, 13–23, DOI: 10.1093/emph/eox025 (2018).
4. Perry, G. H. Evolutionary medicine. *eLife* **10**, e69398, DOI: 10.7554/eLife.69398 (2021).
5. Chmielecki, J. *et al.* Optimization of dosing for egfr-mutant non–small cell lung cancer with evolutionary cancer modeling. *Sci. Transl. Medicine* **3**, DOI: 10.1126/scitranslmed.3002356 (2011).
6. Chakrabarti, S. & Michor, F. Pharmacokinetics and drug interactions determine optimum combination strategies in computational models of cancer evolution. *Cancer Res.* **77**, 3908–3921, DOI: 10.1158/0008-5472.CAN-16-2871 (2017).
7. Maltas, J., Singleton, K. R., Wood, K. C. & Wood, K. B. Drug dependence in cancer is exploitable by optimally constructed treatment holidays. *bioRxiv* DOI: 10.1101/2022.07.01.498458 (2022). https://www.biorxiv.org/content/early/2022/07/03/2022.07.01.498458.full.pdf.
8. Maltas, J. & Wood, K. B. Pervasive and diverse collateral sensitivity profiles inform optimal strategies to limit antibiotic resistance. *PLoS biology* **17**, e3000515 (2019).
9. Iram, S. *et al.* Controlling the speed and trajectory of evolution with counterdiabatic driving. *Nat. Phys.* **17**, 135–142 (2021).
10. Fischer, A., Vázquez-García, I. & Mustonen, V. The value of monitoring to control evolving populations. *Proc. Natl. Acad. Sci.* **112**, 1007–1012 (2015).
11. Poels, K. E. *et al.* Identification of optimal dosing schedules of dacomitinib and osimertinib for a phase i/ii trial in advanced egfr-mutant non-small cell lung cancer. *Nat. Commun.* **12**, 3697, DOI: 10.1038/s41467-021-23912-4 (2021).
12. Weinreich, D. M., Delaney, N. F., DePristo, M. A. & Hartl, D. L. Darwinian Evolution Can Follow Only Very Few Mutational Paths to Fitter Proteins. *Science* **312**, 111–114, DOI: 10.1126/science.1123539 (2006).
13. Goulart, C. P. *et al.* Designing antibiotic cycling strategies by determining and understanding local adaptive landscapes. *PLoS ONE* **8**, e56040, DOI: 10.1371/journal.pone.0056040 (2013).
14. Fragata, I., Blanckaert, A., Dias Louro, M. A., Liberles, D. A. & Bank, C. Evolution in the light of fitness landscape theory. *Trends Ecol. & Evol.* **34**, 69–82, DOI: 10.1016/j.tree.2018.10.009 (2019).
15. Kouyos, R. D. *et al.* Exploring the Complexity of the HIV-1 Fitness Landscape. *PLoS Genet.* **8**, e1002551, DOI: 10.1371/journal.pgen.1002551 (2012).
16. Maltas, J., McNally, D. M. & Wood, K. B. Evolution in alternating environments with tunable interlandscape correlations. *Evolution* **75**, 10–24, DOI: 10.1111/evo.14121 (2021).
17. Gillespie, J. H. Some properties of finite populations experiencing strong selection and weak mutation. *The Am. Nat.* **121**, 691–708 (1983).
18. Watson, C. J. *et al.* The evolutionary dynamics and fitness landscape of clonal hematopoiesis. *Science* **367**, 1449–1454, DOI: 10.1126/science.aay9333 (2020).
19. Gillespie, J. H. Molecular evolution over the mutational landscape. *Evolution* **38**, 1116, DOI: 10.2307/2408444 (1984).
20. Brown, K. M. *et al.* Compensatory mutations restore fitness during the evolution of dihydrofolate reductase. *Mol. Biol. Evol.* **27**, 2682–2690, DOI: 10.1093/molbev/msq160 (2010).
21. Lagator, M., Colegrave, N. & Neve, P. Selection history and epistatic interactions impact dynamics of adaptation to novel environmental stresses. *Proc. Royal Soc. B: Biol. Sci.* **281**, 20141679, DOI: 10.1098/rspb.2014.1679 (2014).
22. Costanzo, M. S., Brown, K. M. & Hartl, D. L. Fitness trade-offs in the evolution of Dihydrofolate reductase and drug resistance in plasmodium falciparum. *PLoS One* **6**, DOI: 10.1371/journal.pone.0019636 (2011).
23. Maisnier-Patin, S. & Andersson, D. I. Adaptation to the deleterious effects of antimicrobial drug resistance mutations by compensatory evolution. *Res. Microbiol.* **155**, 360–369, DOI: 10.1016/j.resmic.2004.01.019 (2004).
24. Farrokhian, N. *et al.* Measuring competitive exclusion in non-small cell lung cancer. *bioRxiv* DOI: 10.1101/2020.09.18.303966 (2020).

25. Merrell, D. J. *The Adaptive Seascape: The Mechanism of Evolution* (University of Minnesota Press, 1994), minne ed. edition edn.

26. Ogbunugafor, C. B., Wylie, C. S., Diakite, I., Weinreich, D. M. & Hartl, D. L. Adaptive Landscape by Environment Interactions Dictate Evolutionary Dynamics in Models of Drug Resistance. *PLoS Comput. Biol.* **12**, 1–20, DOI: 10.1371/journal.pcbi.1004710 (2016).

27. Das, S. G., Direito, S. O., Waclaw, B., Allen, R. J. & Krug, J. Predictable properties of fitness landscapes induced by adaptational tradeoffs. *eLife* **9**, e55155, DOI: 10.7554/eLife.55155 (2020).

28. Mustonen, V. & Lässig, M. From fitness landscapes to seascapes: non-equilibrium dynamics of selection and adaptation. *Trends Genet.* **25**, 111–119, DOI: 10.1016/j.tig.2009.01.002 (2009).

29. Agarwala, A. & Fisher, D. S. Adaptive walks on high-dimensional fitness landscapes and seascapes with distance-dependent statistics. *Theor. Popul. Biol.* **130**, 13–49, DOI: 10.1016/j.tpb.2019.09.011 (2019).

30. Lindsey, H. A., Gallie, J., Taylor, S. & Kerr, B. Evolutionary rescue from extinction is contingent on a lower rate of environmental change. *Nature* **494**, 463–467, DOI: 10.1038/nature11879 (2013).

31. Sorensen, S. V. *et al.* Cost and clinical consequence of antibiotic non-adherence in acute exacerbations of chronic bronchitis. *The Int. J. Tuberc. Lung Dis. The Off. J. Int. Union Against Tuberc. Lung Dis.* **13**, 945–954 (2009).

32. Pechère, J.-C., Hughes, D., Kardas, P. & Cornaglia, G. Non-compliance with antibiotic therapy for acute community infections: a global survey. *Int. J. Antimicrob. Agents* **29**, 245–253, DOI: 10.1016/j.ijantimicag.2006.09.026 (2007).

33. Kardas, P. Patient compliance with antibiotic treatment for respiratory tract infections. *J. Antimicrob. Chemother.* **49**, 897–903, DOI: 10.1093/jac/dkf046 (2002).

34. Swings, T. *et al.* Adaptive tuning of mutation rates allows fast response to lethal stress in escherichia coli. *eLife* **6**, e22939, DOI: 10.7554/eLife.22939 (2017).

35. Gatenby, R. A., Artzy-Randrup, Y., Epstein, T., Reed, D. R. & Brown, J. S. Eradicating metastatic cancer and the eco-evolutionary dynamics of anthropocene extinctions. *Cancer Res.* **80**, 613–623, DOI: 10.1158/0008-5472.CAN-19-1941 (2020).

36. Moreno-Gamez, S. *et al.* Imperfect drug penetration leads to spatial monotherapy and rapid evolution of multidrug resistance. *Proc. Natl. Acad. Sci.* **112**, E2874–E2883, DOI: 10.1073/pnas.1424184112 (2015).

37. Feder, A. F., Harper, K. N., Brumme, C. J. & Pennings, P. S. Understanding patterns of hiv multi-drug resistance through models of temporal and spatial drug heterogeneity. *eLife* **10**, e69032, DOI: 10.7554/eLife.69032 (2021).

38. Kouyos, R. D., Abel zur Wiesch, P. & Bonhoeffer, S. Informed switching strongly decreases the prevalence of antibiotic resistance in hospital wards. *PLoS Comput. Biol.* **7**, e1001094, DOI: 10.1371/journal.pcbi.1001094 (2011).

39. Mira, P. M. *et al.* Rational design of antibiotic treatment plans: A treatment strategy for managing evolution and reversing resistance. *PLOS ONE* **10**, e0122283, DOI: 10.1371/journal.pone.0122283 (2015).

40. Nichol, D. *et al.* Steering evolution with sequential therapy to prevent the emergence of bacterial antibiotic resistance. *PLOS Comput. Biol.* **11**, e1004493, DOI: 10.1371/journal.pcbi.1004493 (2015).

41. Nichol, D. *et al.* Antibiotic collateral sensitivity is contingent on the repeatability of evolution. *Nat. Commun.* **10**, 334, DOI: 10.1038/s41467-018-08098-6 (2019).

42. Kim, S., Lieberman, T. D. & Kishony, R. Alternating antibiotic treatments constrain evolutionary paths to multidrug resistance. *Proc. Natl. Acad. Sci.* **111**, 14494–14499, DOI: 10.1073/pnas.1409800111 (2014).

43. Abel zur Wiesch, P., Kouyos, R., Abel, S., Viechtbauer, W. & Bonhoeffer, S. Cycling empirical antibiotic therapy in hospitals: Meta-analysis and models. *PLoS Pathog.* **10**, e1004225, DOI: 10.1371/journal.ppat.1004225 (2014).

44. Iram, S. *et al.* Controlling the speed and trajectory of evolution with counterdiabatic driving. *Nat. Phys.* **17**, 135–142, DOI: 10.1038/s41567-020-0989-3 (2021).

45. Claxton, A. J., Cramer, J. & Pierce, C. A systematic review of the associations between dose regimens and medication compliance. *Clin. Ther.* **23**, 1296–1310, DOI: 10.1016/S0149-2918(01)80109-0 (2001).

46. Rosenbloom, D. I. S., Hill, A. L., Rabi, S. A., Siliciano, R. F. & Nowak, M. A. Antiretroviral dynamics determines hiv evolution and predicts therapy outcome. *Nat. Medicine* **18**, 1378–1385, DOI: 10.1038/nm.2892 (2012).

47. Engelstädter, J. Fitness landscapes emerging from pharmacodynamic functions in the evolution of multidrug resistance. *J. Evol. Biol.* **27**, 840–853, DOI: 10.1111/jeb.12355 (2014).

48. Zwietering, M. H., Jongenburger, I., Rombouts, F. M. & van 't Riet, K. Modeling of the bacterial growth curve. *Appl. Environ. Microbiol.* **56**, 1875–1881, DOI: 10.1128/aem.56.6.1875-1881.1990 (1990).

49. Gonidakis, S. & Longo, V. D. Assessing chronological aging in bacteria. *Methods Mol. Biol.* **965**, 421–437, DOI: 10.1007/978-1-62703-239-1_28 (2013).

50. Jee, J. *et al.* Rates and mechanisms of bacterial mutagenesis from maximum-depth sequencing. *Nature* **534**, 693–696, DOI: 10.1038/nature18313 (2016).

51. Patel, K. B., Nicolau, D. P., Nightingale, C. H. & Quintiliani, R. Pharmacokinetics of cefotaxime in healthy volunteers and patients. *Diagn. Microbiol. Infect. Dis.* **22**, 49–55, DOI: 10.1016/0732-8893(95)00072-I (1995).

Additional Information

Acknowledgements

We would like to thank the Weinreich Lab at Brown University for providing the genetically engineered *E. coli* strains used in this work. This work was made possible by the National Institute of Health (5R37CA244613-03, 5T32GM007250-46, and T32CA09418) and American Cancer Society Research Scholar Grant (RSG-20-096-01). Figures 3 and 7 created with BioRender.com.

Author Contributions

Eshan King: Conceptualization, experimental design, software development, *in vitro* experiments, computational experiments, data analysis, visualization, writing (original draft and editing). Jeff Maltas: Conceptualization, experimental design, *in vitro* experiments, writing (editing). Davis T. Weaver: Software development, writing (editing). Rowan Barker-Clarke: Conceptualization, experimental design, writing (editing). Julia Pelesko: *in vitro* experiments. Emily Dolson: Conceptualization, experimental design, writing (editing). Jacob G. Scott: Conceptualization, supervision, experimental design, writing (editing).

Supplemental Materials

Experimental data

We measured an empirical fitness seascape by measuring genotype-specific *E. coli* dose-response curves to cefotaxime. After obtaining growth rates for each genotype-drug concentration combination, we fit Hill dose-response curves to growth rate versus drug concentration data for each genotype. The data and corresponding curve fits are shown in **Fig. S1**.

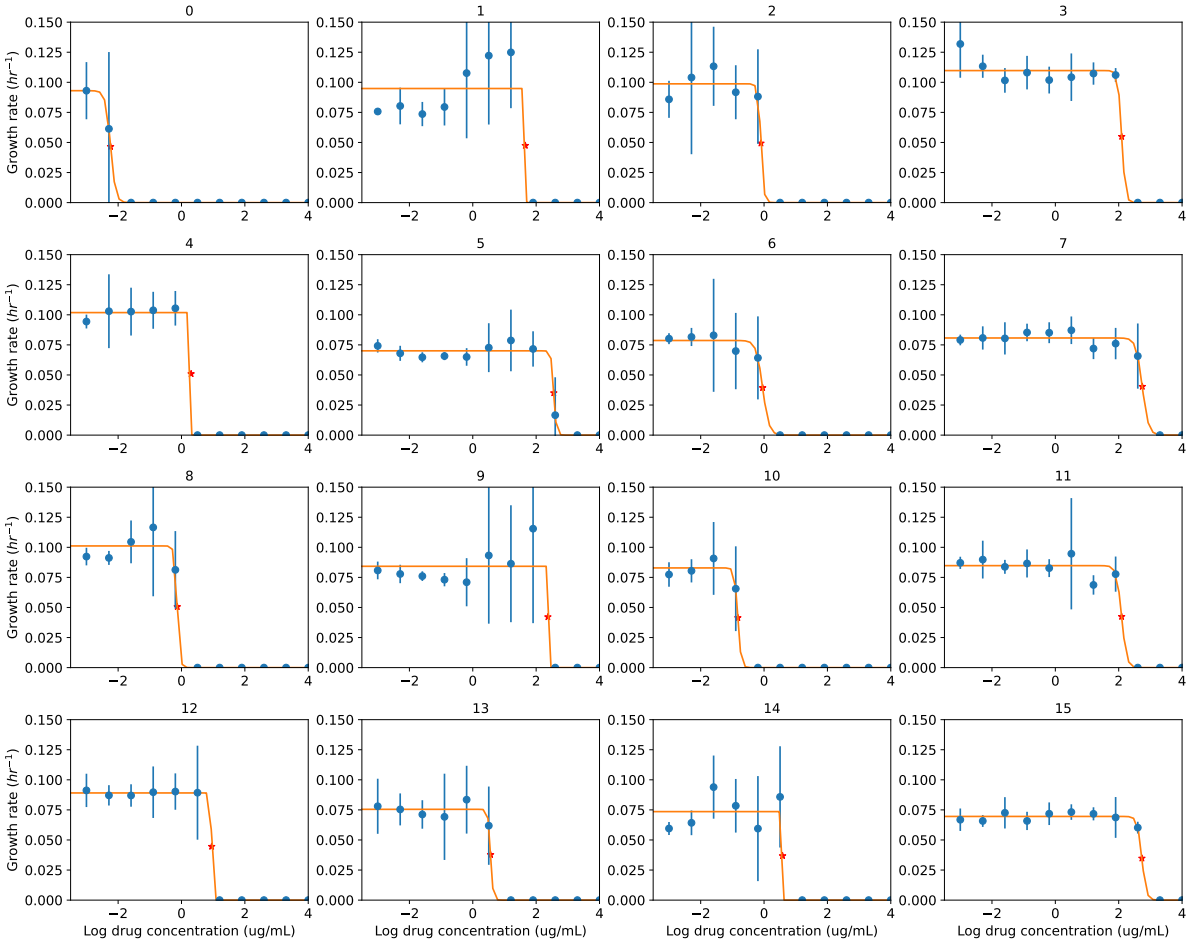

Figure S1. Dose-response curve fits used to parameterize the fitness seascape. Red star indicates estimated genotype-specific IC_{50}. Panels are labeled with the genotype number in base 10.

Using data from this experiment, we compared our estimated IC_{50} to the MIC reported by Weinreich et al.[12] in the same engineered *E. coli* samples. We found a linear correlation between both experiments, with $r = 0.744$, $p < 0.001$ (Pearson correlation) (**Fig. S2**).

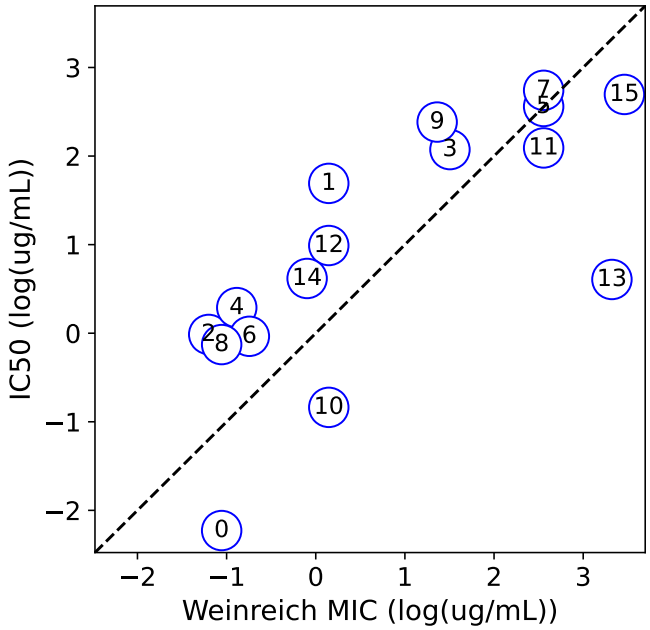

Figure S2. Comparison between observed IC_{50} and MIC reported by Weinreich et al.[12]. Numbers within the circles are genotype number in base 10. Correlation coefficient $r = 0.744$, $p < 0.001$.

Evolutionary tradeoffs

We further sought to investigate evolutionary trade-offs, or fitness costs to resistance, by plotting the genotype-specific drug-free growth rate against the IC_{50}, hypothesizing that there would be an inverse relationship as metabolic costs to resistance limit growth rate. We found a roughly inverse relationship (**Fig. S3**), however this was not statistically significant ($r = -0.34$, $p = 0.19$, Spearman rank-correlation). We also qualitatively noted that the number of mutations was proportional to the IC_{50} and inversely proportional to the growth rate.

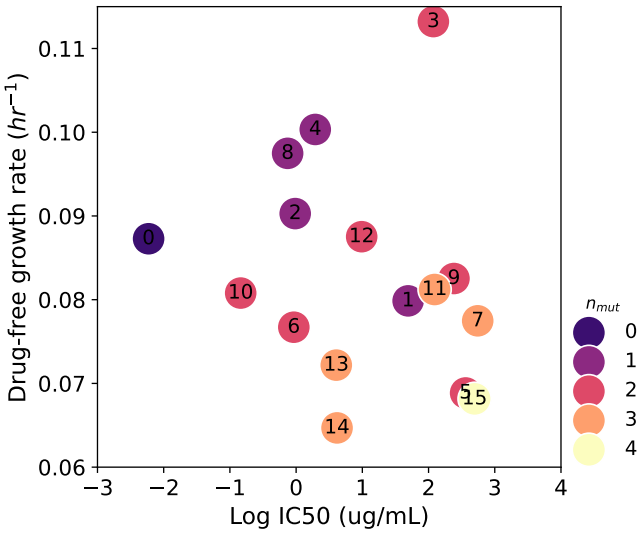

Figure S3. **Genotype-specific IC_{50} versus drugless growth rate.** Numbers within the circles are genotype number in base 10. Colors indicate the number of mutations.

To further investigate the impact of the number of mutations on growth rate and drug sensitivity, we plotted drug-free growth rate and IC_{50} against the number of mutations for each strain (**Fig. S4**). We found a statistically significant inverse relationship between growth rate and mutations ($r^2 = 0.31, p = 0.025$) and a significant positive relationship between IC_{50} and mutations ($r^2 = 0.4, p = 0.009$). These results demonstrate that resistance-conferring mutations impart a penalty on drug-free growth rate, further illustrating the presence of fitness trade-offs in this system.

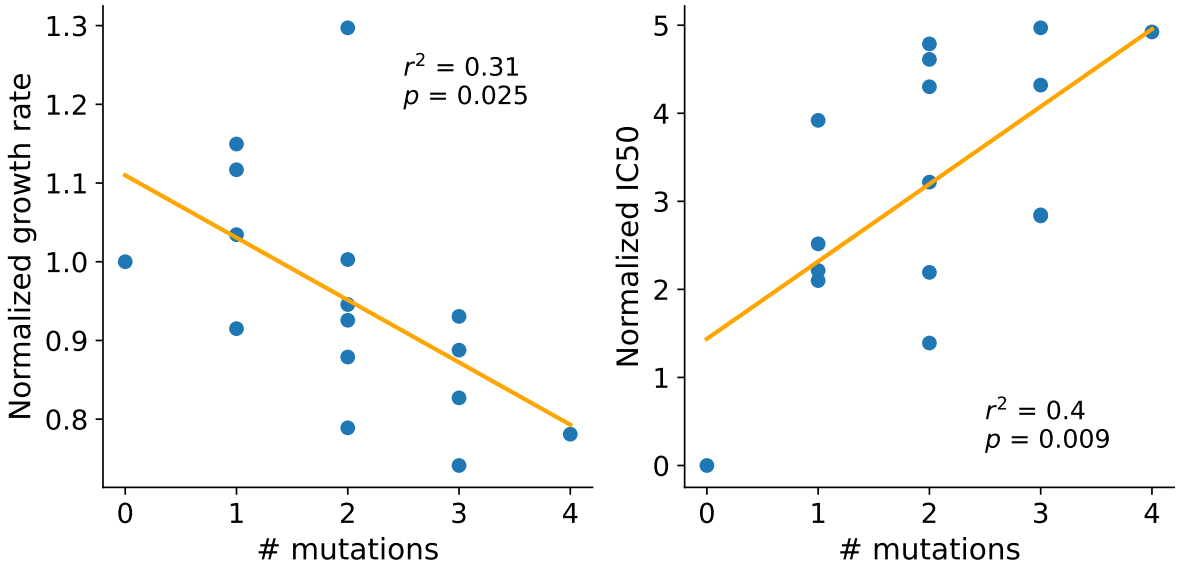

Figure S4. Relationship between number of mutations and evolutionary trade-offs. Left: Association between number of mutations and drug-free growth rate. **Right:** Relationship between number of mutations and IC_{50}. Orange line is linear regression fit. Growth rate and IC_{50} are normalized to the wild-type (strain 0000).

Parameter sensitivity analysis

Finally, we investigated the generalizability of our evolutionary model by performing a parameter sensitivity analysis. We observed the impact of death rate, mutation rate, and carrying capacity on the probability of survival for a fixed rate of environmental change. We found that mutation rate and carrying capacity dramatically impact the probability of survival, while death rate does not substantively impact survival (**Fig . S5**). Results of a multiple linear regression are shown in **Table S1**.

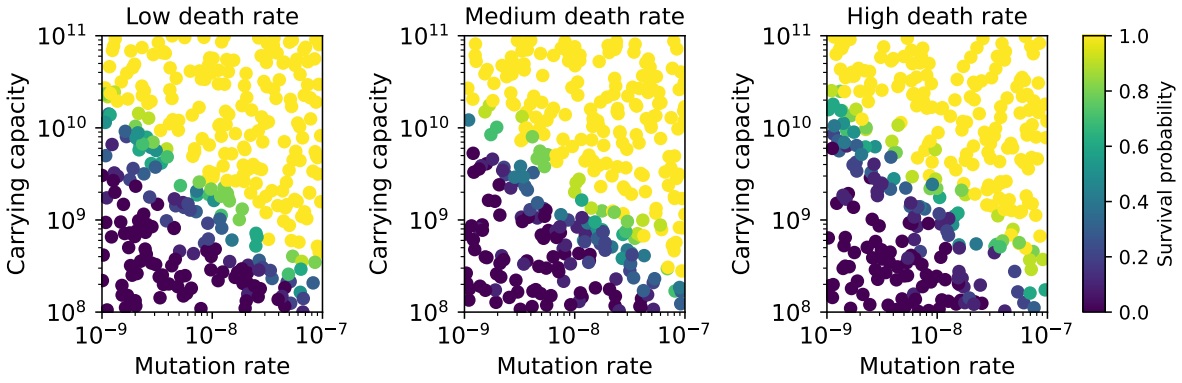

Figure S5. Sensitivity analysis reveals model sensitivity to mutation rate and carrying capacity Low death rate is <= 0.034 per hour, medium death rate is > 0.034 and <= 0.068, and high death rate is > 0.068 and <= 0.1 (all in units of hr^{-1}).

	Coefficients	*P-value*	*Lower 95%*	*Upper 95%*
Intercept	0.353714781	6.04668E-43	0.30557497	0.40185459
death rate	-0.000270987	0.994233931	-0.0738362	0.07329426
mutation rate	0.646747572	2.0296E-46	0.56256774	0.7309274
carrying capacity	0.955545458	5.1096E-77	0.86323011	1.0478608

Table S1. Results of multiple linear regression show model sensitivity to mutation rate and carrying capacity.